CHAPTER 2

AN INVESTIGATION ON TEMPERATURE-RATE DEPENDENT THERMOELASTICITY USING A COMPLETE FINITE ELEMENT APPROACH

2.1 Introduction[1]

The present chapter aims at studying a thermoelastic problem under the temperature-rate dependent theory by considering a hollow disk with the thermal shock applied on its inner boundary. The motivation of this chapter is further oriented to describe how a complete finite element scheme can be applied to solve the problems of coupled dynamical thermoelasticity.

Deriving a closed form solution for the system of coupled thermoelastic equations is possible only for a few initial boundary value problems, and closed form solution cannot be obtained for many practical problems. Due to this reason and to reduce the complexity of the problem, some simplified forms of basic equations are assumed by observations based on practical experiments. In the structural designs, the use of these approximated forms of basic equations may result good for simple structures, but for heavy-duty equipment, it does not give satisfactory responses. Hence, the calculation must be performed on the basis of all governing equations of thermoelasticity theory in such cases. Usually, numerical methods like finite difference, finite element and

[1]Part of this chapter is published in *Computational Methos in Science and Technology*, Vol. 25(2), pp. 61-70, 2019.

boundary element methods are used in these cases. Analysis of thermoelastic responses for various problems by using the finite difference schemes has been reported by the researchers including Barone and Patterson (1998), Abd-Alla and Mahmoud (2010), Lee et al. (2001). The boundary element method has been applied by Chen and Dargush (1995), Hetnarski and Eslami (2009), Hosseini and Eslami (2000), Sladek and Sladek (1984) to solve different coupled and uncoupled thermoelastic problems. However, it has been realized that among all the numerical methods, the finite element method (FEM) can be applied efficiently to various coupled thermoelastic problems (see Prakash et al. (2000), Mishra et al. (2008) and Xu and Li (2003)). The finite element formulation for spatial derivatives with a time integration scheme is the most widely used numerical method for structural problems involving thermomechanical loading. In this approach, the Laplace transformation technique is generally applied for the time domain, and then the finite element equation is derived for the space domain to get the solution in Laplace transform domain. Further, the suitable method for numerical inversion of the transformed solution gives the final solution of the coupled equations. A problem of the hollow disc for various thermoelasticity models using FEM with Laplace transformation has been studied by Bagri and Eslami (2008), Hetnarski and Eslami (2009) and also by Kothari and Mukhopadhyay (2013). Hasanpour and Mirzaei (2018), Hosseini (2009), Sladek et al. (2001) have solved different thermoelastic problems using meshless techniques with the Newmark method as well as with the implicit central difference scheme. Rincon et al. (2005) have discussed an alternative approach for the time domain to solve coupled thermoelastic equations using the finite element method. They have suggested the discretization in space for deriving finite element equations and then used an implicit Newmark scheme to get the solution in the time domain. Abbas and Alzahrani (2018) have used FEM with implicit temporal integration method to solve a mode-I crack problem in a two dimensional isotropic medium based on GN thermoelasticity theory. Stasa (1985) has given a detailed discussion for FEM to various

structural problems and suggested a complete finite element approach for space as well as time domain. Balla (1989) derived the explicit formulation of field variables for a two dimensional heat conduction equation based on the CV model using this approach.

This Chapter attempts to apply the complete Galerkin's approach of finite element for the solution of problems on the coupled dynamical thermoelasticity theory. It aims to investigate the predictions of the temperature-rate dependent thermoelasticity theory (GL theory) as compared to the LS thermoelasticity theory (Lord and Shulman (1967)). Here, the unified form of thermoelasticity theories proposed by Lord and Shulman (1967) and Green and Lindsay (1972) are employed by considering a problem of hollow disk subjected to a thermal shock applied on its inner boundary. In order to solve this radially symmetric problem, first, the space domain is discretized into small elements of equal intervals, and then the weak formulation is used to derive the finite element equations for the space domain. Next, the discretization of the time domain is used to apply Galerkin's approach of finite element and derived explicit finite element equations for the time and space domain. The implementation of the scheme is performed for a particular case, and computational work is carried out to obtain the numerical solution of the problem. For the validation of results, the present solution is compared with the solutions obtained by a trans-FEM method in which the Laplace transform technique is used for the time domain. It is observed that there is a perfect match in solutions by the complete finite element approach with the corresponding solution obtained by a trans-finite element method which implies successful implementation of the present scheme. The variations of all field variables are studied for the thermoelasticity theory involving two thermal relaxation parameters (temperature-rate dependent theory) and thermoelasticity theory with one relaxation parameter (LS theory). A comparative analysis is made for the predictions by two different theories.

2.2 Basic Governing Equations

Following Lord and Shulman (1967) and Green and Lindsay (1972), the unified form of the basic governing equations corresponding to LS and GL thermoelasticity theories for a homogeneous and isotropic medium can be given as follows:

The stress-displacement equation of motion in absence of any body force:

$$\sigma_{ij,j} = \rho \ddot{u}_i. \tag{2.2.1}$$

The energy balance equation without heat source:

$$q_{i,i} = -\rho T_0 \dot{S}. \tag{2.2.2}$$

The constitutive relations:

$$\sigma_{ij} = 2\mu\varepsilon_{ij} + \lambda\varepsilon_{kk}\delta_{ij} - \beta(\theta + mt_1\dot{\theta})\delta_{ij}, \tag{2.2.3}$$

$$T_0\rho S = \rho c_E(\theta + mt_2\dot{\theta}) + T_0\beta e_{kk}, \tag{2.2.4}$$

$$q_i + nt_q\frac{\partial q_i}{\partial t} = -K\theta_{,i}. \tag{2.2.5}$$

Strain-displacement relation:

$$e_{ij} = \frac{1}{2}(u_{i,j} + u_{j,i}). \tag{2.2.6}$$

In this system of equations, a rectangular coordinate system x_k in three dimensional Euclidean space with usual indicial notations and m, n as parameters are used for unifying the governing equations corresponding to LS and GL theories such that the equations of respective theories can be obtained by setting the values of the parameters m, n as follows:

- **For LS theory:** $m = 0, n = 1$
- **For GL theory:** $m = 1, n = 0$.

Therefore, the unified heat conduction equation can be obtained from Eqs. (2.2.2), (2.2.4) and (2.2.5) as

$$\left(1+nt_q\frac{\partial}{\partial t}\right)\left[\rho c_E(1+mt_2\frac{\partial}{\partial t})\dot{\theta}+\beta T_0\dot{\varepsilon}_{kk}\right]=K\theta_{,ii}. \tag{2.2.7}$$

2.3 Problem Formulation

In the present work, we consider a problem of a hollow disk with inner radius, r_1 and outer radius r_2 under the linear thermoelasticity theory based on LS and GL model as described above. The material of the disc is assumed to be homogeneous and isotropic for this problem. Let us assume radially symmetric motion of the body so that the physical field variables are functions of the radial coordinate, r and time, t only. Hence, the displacement vector has only the radial component, $u\,(r,t)$. Therefore, the Eq. (2.2.7) for the present problem can be written in the polar form as

$$K\left(\frac{\partial^2\theta}{\partial r^2}+\frac{1}{r}\frac{\partial\theta}{\partial r}\right)-\left(1+nt_q\frac{\partial}{\partial t}\right)\left[\rho c_E(1+mt_2\frac{\partial}{\partial t})\frac{\partial\theta}{\partial t}+\beta T_0\frac{\partial}{\partial t}\left(\frac{\partial u}{\partial r}+\frac{u}{r}\right)\right]=0. \tag{2.3.1}$$

Further, from Eqs. (2.2.1) and (2.2.3), the polar form of the equation of motion in terms of displacement and temperature is obtained as

$$(\lambda+2\mu)\left[\frac{\partial^2 u}{\partial r^2}+\frac{1}{r}\frac{\partial u}{\partial r}-\frac{u}{r^2}\right]-\beta\left(\frac{\partial\theta}{\partial r}+mt_1\frac{\partial\dot{\theta}}{\partial r}\right)-\rho\frac{\partial^2 u}{\partial t^2}=0. \tag{2.3.2}$$

The radial and circumference stress components can also be obtained from Eq. (2.2.3) as

$$\sigma_{rr}=2\mu\frac{\partial u}{\partial r}+\lambda\left(\frac{\partial u}{\partial r}+\frac{u}{r}\right)-\beta\left(\theta+mt_1\dot{\theta}\right), \tag{2.3.3}$$

$$\sigma_{\phi\phi}=2\mu\frac{u}{r}+\lambda\left(\frac{\partial u}{\partial r}+\frac{u}{r}\right)-\beta\left(\theta+mt_1\dot{\theta}\right), \tag{2.3.4}$$

where σ_{rr} and $\sigma_{\phi\phi}$ are radial and circumferential stress components, respectively.

For this problem, the frictionless inner surface is considered, and a thermal shock is

applied to the inner boundary of the disk. The rigid outer boundary is assumed to be insulated. Also, the initial conditions are considered to be homogeneous. Therefore, we have

$$\left.\begin{aligned} u(r,0)=0,\ \theta(r,0)=0,\ \text{at } r_1\le r\le r_2 \\ \dot{u}(r,0)=0,\ \dot{\theta}(r,0)=0,\ \text{at } r_1\le r\le r_2 \end{aligned}\right\}, \tag{2.3.5}$$

$$\left.\begin{aligned} \theta(r_1,t)=1-e^{-1000t} \quad \text{and } \sigma_{rr}(r_1,t)=0, \quad \text{at } t>0 \\ \tfrac{\partial\theta(r_2,t)}{\partial r}=0, \qquad \text{and } u(r_2,0)=0, \quad \text{at } t>0 \end{aligned}\right\}. \tag{2.3.6}$$

Now, to make the equations in simplified non-dimensional forms, the following dimensionless variables are assumed:

$$r'=c_1n_0r,\ \theta'=\tfrac{\theta}{T_0},\ t'=c_1^2n_0t,\ (t'_q,t'_1,t'_2)=c_1^2n_0(t_q,t_1,t_2),$$

$$(\sigma'_{rr},\sigma'_{\phi\phi})=(\tfrac{\sigma_{rr}}{\beta T_0},\tfrac{\sigma_{\phi\phi}}{\beta T_0}),\ \ u'=\tfrac{c_1n_0(\lambda+2\mu)}{\beta T_0}u,\ c_1^2=\tfrac{(\lambda+2\mu)}{\rho},\ n_0=\tfrac{\rho c_E}{K}.$$

Using the above dimensionless variables and ignoring the prime notations for simplicity, we find that the basic Eqs. (2.3.1 - 2.3.4) will take the following forms:

$$(\lambda+2\mu)\left[\frac{\partial^2u}{\partial r^2}+\frac{1}{r}\frac{\partial u}{\partial r}-\frac{u}{r^2}\right]-(\lambda+2\mu)\left(\frac{\partial\theta}{\partial r}+mt_1\frac{\partial\dot{\theta}}{\partial r}\right)-\rho c_1^2\frac{\partial^2u}{\partial t^2}=0, \tag{2.3.7}$$

$$\frac{\partial^2\theta}{\partial r^2}+\frac{1}{r}\frac{\partial\theta}{\partial r}-\left(1+(nt_q+mt_2)\frac{\partial}{\partial t}\right)\frac{\partial}{\partial t}\left[\theta+\xi\left(\frac{\partial u}{\partial r}+\frac{u}{r}\right)\right]=0, \tag{2.3.8}$$

$$\sigma_{rr}=\frac{2\mu}{\lambda+2\mu}\frac{\partial u}{\partial r}+\frac{\lambda}{\lambda+2\mu}\left(\frac{\partial u}{\partial r}+\frac{u}{r}\right)-\left(\theta+mt_1\dot{\theta}\right), \tag{2.3.9}$$

$$\sigma_{\phi\phi}=\frac{2\mu}{\lambda+2\mu}\frac{u}{r}+\frac{\lambda}{\lambda+2\mu}\left(\frac{\partial u}{\partial r}+\frac{u}{r}\right)-\left(\theta+mt_1\dot{\theta}\right). \tag{2.3.10}$$

where $\xi=\frac{\beta^2T_0}{\rho c_E(\lambda+2\mu)}$.

2.4 Finite Element Formulation

Now, to solve the coupled Eqs. (2.3.7) and (2.3.8) with the initial conditions (2.3.5) and boundary conditions (2.3.6), the Galerkin's approach of complete finite element

method is used. In this process, discretization of space domain into small sub-domains takes place (see Fig. 2.4.1), and the temperature and displacement are approximated by the following functions for each sub-domain:

$$u = \sum_{i=1}^{h} N_i U_i^{(e)}(t), \text{ and } \theta = \sum_{i=1}^{h} N_i \Theta_i^{(e)}(t), \tag{2.4.1}$$

where N_i, $i = 1, 2, ..h$ are the shape functions and $U_i^{(e)}(t), \Theta_i^{(e)}(t)$, $i = 1, 2, ..h$ are the the approximated nodal displacement and temperature, respectively.

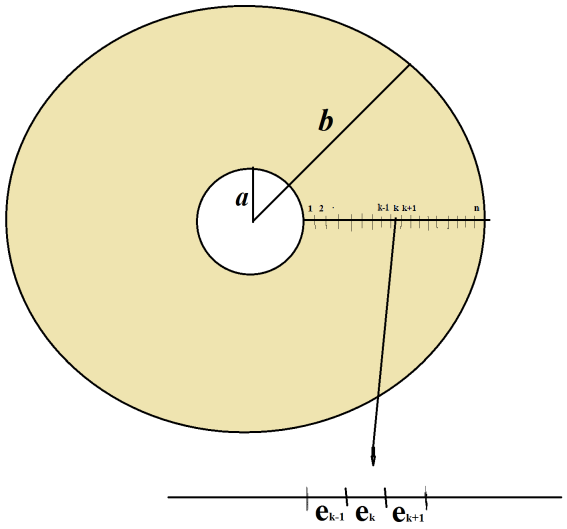

Figure 2.4.1: Finite element profile

Therefore, by applying Galerkin's approach and assuming shape function as weight function with the approximation (2.4.1), the Eqs. (2.3.7) and (2.3.8) can be written in the forms

$$\int_V N_i \left[(\lambda + 2\mu) \left[\frac{\partial^2 u}{\partial r^2} + \frac{1}{r}\frac{\partial u}{\partial r} - \frac{u}{r^2} \right] - (\lambda + 2\mu) \left(\frac{\partial \theta}{\partial r} + m t_1 \frac{\partial \dot{\theta}}{\partial r} \right) - \rho c_1^2 \frac{\partial^2 u}{\partial t^2} \right] dV = 0, \tag{2.4.2}$$

$$\int_V N_i \left[\left(\frac{\partial^2 \theta}{\partial r^2} + \frac{1}{r}\frac{\partial \theta}{\partial r} \right) - \left(1 + (n t_q + m t_2) \frac{\partial}{\partial t} \right) \frac{\partial}{\partial t} \left[\theta + \xi \left(\frac{\partial u}{\partial r} + \frac{u}{r} \right) \right] \right] dV = 0. \tag{2.4.3}$$

For a disk, the infinitesimal volume element will be $rdrd\phi$, but in the present case of radial symmetry, all the variables are independent from the angle. Therefore, by

considering the infinitesimal volume element as $dV = rdr$ and $r = r_k + \eta$, $k = 1, 2, ...h$ in the Eqs. (2.4.2) and (2.4.3), we have

$$\int_0^h N_i \left[(\lambda + 2\mu) \left[\frac{\partial^2 u}{\partial \eta^2} + \frac{1}{(\eta + r_i)} \frac{\partial u}{\partial \eta} - \frac{u}{(\eta + r_i)^2} \right] \right. \\ \left. - (\lambda + 2\mu) \left(\frac{\partial \theta}{\partial \eta} + m t_1 \frac{\partial \dot{\theta}}{\partial \eta} \right) - \rho c_1^2 \frac{\partial^2 u}{\partial t^2} \right] (\eta + r_i) d\eta = 0, \tag{2.4.4}$$

and

$$\int_0^h N_i \left[\left(\frac{\partial^2 \theta}{\partial \eta^2} + \frac{1}{(\eta + r_k)} \frac{\partial \theta}{\partial \eta} \right) - \left(1 + (n t_q + m t_2) \frac{\partial}{\partial t} \right) \left[\frac{\partial \theta}{\partial t} \right. \right. = 0 \\ \left. \left. - \xi \frac{\partial}{\partial t} \left(\frac{\partial u}{\partial \eta} + \frac{u}{(\eta + r_k)} \right) \right] \right] (\eta + r_k) d\eta. \tag{2.4.5}$$

Now, we apply integration by parts in the first term of the Eq. (2.4.4) to derive the weak formulation, which implies that

$$\int_0^h \left[(\lambda + 2\mu) \left((\eta + r_k) \frac{\partial N_i}{\partial \eta} \frac{\partial u}{\partial \eta} + N_i \frac{u}{(\eta + r_k)} \right) + \rho c_1^2 N_i \frac{\partial^2 u}{\partial t^2} \right] d\eta \\ + \int_0^h N_i (\lambda + 2\mu) \left(\frac{\partial \theta}{\partial \eta} + m t_1 \frac{\partial \dot{\theta}}{\partial \eta} \right) (\eta + r_k) d\eta = (\lambda + 2\mu)(\eta + r_k) N_i |_0^h . \tag{2.4.6}$$

Similarly, the Eq. (2.4.5) yields

$$\int_0^h \frac{\partial N_i}{\partial \eta} \frac{\partial \theta}{\partial \eta} (\eta + r_k) d\eta + \int_0^h N_i (\eta + r_k) \left(1 + (n t_q + m t_2) \frac{\partial}{\partial t} \right) \frac{\partial \theta}{\partial t} d\eta \\ + \int_0^h \xi \left(1 + n t_q \frac{\partial}{\partial t} \right) \frac{\partial}{\partial t} \left(\frac{\partial u}{\partial r} + \frac{u}{r} \right) N_i d\eta = N_i \frac{\partial \theta}{\partial \eta} (\eta + r_k) \Big|_0^h . \tag{2.4.7}$$

Now, using the Eq. (2.4.1) in Eqs. (2.4.6) and (2.4.7) for $i = 1, 2$, the finite element equation formulation is obtained as

$$\begin{aligned}
&U_1^{(e)}(\lambda+2\mu)\int_0^h\left[(\eta+r_k)\frac{\partial N_i}{\partial\eta}\frac{\partial N_1}{\partial\eta}+\frac{N_iN_1}{(\eta+r_k)}\right]d\eta+\Theta_1^{(e)}(\lambda+2\mu)\int_0^h N_i\frac{\partial N_1}{\partial\eta}(\eta+r_k)d\eta\\
&+U_2^{(e)}(\lambda+2\mu)\int_0^h\left[(\eta+r_k)\frac{\partial N_i}{\partial\eta}\frac{\partial N_2}{\partial\eta}+\frac{N_iN_2}{(\eta+r_k)}\right]d\eta+\Theta_2^{(e)}(\lambda+2\mu)\int_0^h N_i\frac{\partial N_2}{\partial\eta}(\eta+r_k)d\eta\\
&+\dot{\Theta}_1^{(e)}\left[mt_1(\lambda+2\mu)\int_0^h N_i\frac{\partial N_1}{\partial\eta}(\eta+r_k)d\eta\right]+\dot{\Theta}_2^{(e)}\left[mt_1(\lambda+2\mu)\int_0^h N_i\frac{\partial N_2}{\partial\eta}(\eta+r_k)d\eta\right]\\
&+\ddot{U}_1^{(e)}\left[\int_0^h\rho c_1^2N_iN_1d\eta\right]+\ddot{U}_2^{(e)}\left[\int_0^h\rho c_1^2N_iN_2d\eta\right]=(\lambda+2\mu)N_i\frac{\partial u}{\partial\eta}(\eta+r_k)\Big|_{r_k}^{r_{k+1}},
\end{aligned}\tag{2.4.8}$$

$$\begin{aligned}
&\Theta_1^{(e)}\left[\int_0^h\frac{\partial N_i}{\partial\eta}\frac{\partial N_1}{\partial\eta}(\eta+r_k)d\eta\right]+\Theta_2^{(e)}\left[\int_0^h\frac{\partial N_i}{\partial\eta}\frac{\partial N_2}{\partial\eta}(\eta+r_k)d\eta\right]\\
&+\dot{\Theta}_1^{(e)}\left[\int_0^h N_iN_1(\eta+r_k)d\eta\right]+\dot{\Theta}_2^{(e)}\left[\int_0^h N_iN_2(\eta+r_k)d\eta\right]\\
&+\ddot{\Theta}_1^{(e)}\left[(nt_q+mt_2)\int_0^h N_iN_1(\eta+r_k)d\eta\right]\\
&+\ddot{\Theta}_2^{(e)}\left[(nt_q+mt_2)\int_0^h N_iN_2(\eta+r_k)d\eta\right]\\
&+\dot{U}_1^{(e)}\left[\xi\int_0^h N_i(\eta+r_k)\left(\frac{\partial N_1}{\partial\eta}+\frac{N_1}{(\eta+r_k)}\right)d\eta\right]+\\
&\dot{U}_2^{(e)}\left[\xi\int_0^h N_i(\eta+r_k)\left(\frac{\partial N_2}{\partial\eta}+\frac{N_2}{(\eta+r_k)}\right)d\eta\right]\\
&+\ddot{U}_1^{(e)}\left[nt_q\xi\int_0^h N_i(\eta+r_k)\left(\frac{\partial N_1}{\partial\eta}+\frac{N_1}{(\eta+r_k)}\right)d\eta\right]\\
&+\ddot{U}_2^{(e)}\left[nt_q\xi\int_0^h N_i(\eta+r_k)\left(\frac{\partial N_2}{\partial\eta}+\frac{N_2}{(\eta+r_k)}\right)d\eta\right]=\frac{\partial\theta}{\partial\eta}N_i(\eta+r_k)\Big|_{r_k}^{r_{k+1}}.
\end{aligned}\tag{2.4.9}$$

Therefore, in view of Eqs. (2.4.8) and (2.4.9), the matrix form of finite element equation

for a single element can be obtained as

$$\begin{bmatrix} [R_{11}] & [R_{12}] \\ [R_{21}] & [R_{22}] \end{bmatrix} \begin{bmatrix} \ddot{U}_1 \\ \ddot{\Theta}_1 \\ \ddot{U}_2 \\ \ddot{\Theta}_2 \end{bmatrix}^{(e)} + \begin{bmatrix} [Q_{11}] & [Q_{12}] \\ [Q_{21}] & [Q_{22}] \end{bmatrix} \begin{bmatrix} \dot{U}_1 \\ \dot{\Theta}_1 \\ \dot{U}_2 \\ \dot{\Theta}_2 \end{bmatrix}^{(e)} + \tag{2.4.10}$$

$$\begin{bmatrix} [P_{11}] & [P_{12}] \\ [P_{21}] & [P_{22}] \end{bmatrix} \begin{bmatrix} U_1 \\ \Theta_2 \\ U_1 \\ \Theta_2 \end{bmatrix}^{(e)} = \begin{bmatrix} J_1 \\ g_1 \\ J_2 \\ g_2 \end{bmatrix}^{(e)},$$

where

$$\left.\begin{aligned} [P_{11}] &= \begin{bmatrix} A_{11}^{11} & A_{11}^{12} \\ A_{11}^{21} & A_{11}^{22} \end{bmatrix}, [P_{12}] = \begin{bmatrix} A_{12}^{11} & A_{12}^{12} \\ A_{12}^{21} & A_{12}^{22} \end{bmatrix}, [P_{21}] = \begin{bmatrix} A_{21}^{11} & A_{21}^{12} \\ A_{21}^{21} & A_{21}^{22} \end{bmatrix}, \\ [P_{22}] &= \begin{bmatrix} A_{22}^{11} & A_{22}^{12} \\ A_{22}^{21} & A_{22}^{22} \end{bmatrix}, [Q_{11}] = \begin{bmatrix} \dot{A}_{11}^{11} & \dot{A}_{11}^{12} \\ \dot{A}_{11}^{21} & \dot{A}_{11}^{22} \end{bmatrix}, [P_{12}] = \begin{bmatrix} \dot{A}_{12}^{11} & \dot{A}_{12}^{12} \\ \dot{A}_{12}^{21} & \dot{A}_{12}^{22} \end{bmatrix}, \\ [Q_{21}] &= \begin{bmatrix} \dot{A}_{21}^{11} & \dot{A}_{21}^{12} \\ \dot{A}_{21}^{21} & \dot{A}_{21}^{22} \end{bmatrix}, [Q_{22}] = \begin{bmatrix} \dot{A}_{22}^{11} & \dot{A}_{22}^{12} \\ \dot{A}_{22}^{21} & \dot{A}_{22}^{22} \end{bmatrix}, [R_{11}] = \begin{bmatrix} \ddot{A}_{11}^{11} & \ddot{A}_{11}^{12} \\ \ddot{A}_{11}^{21} & \ddot{A}_{11}^{22} \end{bmatrix}, \\ [R_{12}] &= \begin{bmatrix} \ddot{A}_{12}^{11} & \ddot{A}_{12}^{12} \\ \ddot{A}_{12}^{21} & \ddot{A}_{12}^{22} \end{bmatrix}, [R_{21}] = \begin{bmatrix} \ddot{A}_{21}^{11} & \ddot{A}_{21}^{12} \\ \ddot{A}_{21}^{21} & \ddot{A}_{21}^{22} \end{bmatrix}, [R_{22}] = \begin{bmatrix} \ddot{A}_{22}^{11} & \ddot{A}_{22}^{12} \\ A_{22}^{21} & \ddot{A}_{22}^{22} \end{bmatrix} \end{aligned}\right\}, \tag{2.4.11}$$

with

$$\left.\begin{array}{c} A_{ij}^{11}=\left[(\lambda+2\mu)\int_0^h\left[(\eta+r_k)\frac{\partial N_i}{\partial\eta}\frac{\partial N_j}{\partial\eta}+\frac{N_iN_j}{(\eta+r_k)}\right]d\eta\right],\ \dot{A}_{ij}^{11}=0,\\ \ddot{A}_{ij}^{11}=\left[\int_0^h\rho c_1^2N_iN_jd\eta\right],\ A_{ij}^{12}=\left[(\lambda+2\mu)\int_0^h N_i\frac{\partial N_j}{\partial\eta}(\eta+r_k)d\eta\right],\\ \dot{A}_{ij}^{12}=mt_1\left[(\lambda+2\mu)\int_0^h N_i\frac{\partial N_j}{\partial\eta}(\eta+r_k)d\eta\right],\ \ddot{A}_{ij}^{12}=0,\ A_{ij}^{21}=0,\\ \dot{A}_{ij}^{21}=\left[\xi\int_0^h N_i(\eta+r_k)\left(\frac{\partial N_j}{\partial\eta}+\frac{N_j}{(\eta+r_k)}\right)d\eta\right],\\ \ddot{A}_{ij}^{21}=\left[\int_0^h nt_q\xi\left[\frac{\partial N_j}{\partial\eta}N_i+\frac{N_iN_j}{(\eta+r_k)}\right](\eta+r_k)d\eta\right]\\ A_{ij}^{22}=\left[\int_0^h\frac{\partial N_i}{\partial\eta}\frac{\partial N_j}{\partial\eta}(\eta+r_k)d\eta\right],\ \dot{A}_{ij}^{22}=\left[\int_0^h(\eta+r_k)N_iN_jd\eta\right],\\ \ddot{A}_{ij}^{12}=\left[(nt_q+mt_2)\int_0^h N_iN_j(\eta+r_k)d\eta\right] \end{array}\right\}. \tag{2.4.12}$$

Also, the load vector can be written as

$$\left.\begin{array}{cc} J_1=-(\lambda+2\mu)\frac{\partial u}{\partial\eta}(\eta+r_k)\Big|_{r_k}, & J_2=(\lambda+2\mu)\frac{\partial u}{\partial\eta}(\eta+r_k)\Big|_{r_{k+1}}\\ g_1=-\frac{\partial\theta}{\partial\eta}(\eta+r_k)\Big|_{r_k}, & g_2=\frac{\partial\theta}{\partial\eta}N_i(\eta+r_k)\Big|_{r_{k+1}} \end{array}\right\}. \tag{2.4.13}$$

Hence, from Eqs. (2.4.10-2.4.13) and the boundary conditions (2.3.5-2.3.6), the global system of differential equations for the whole disk are written in the matrix form as

$$R\ddot{\Omega}+Q\dot{\Omega}+P\Omega=f, \tag{2.4.14}$$

where, $f=\begin{Bmatrix}\lambda U_1-(\lambda+2\mu)\theta_1\\0\\0\\.\\.\\0\end{Bmatrix}_{(h-2)\times1}$, $\Omega=\begin{Bmatrix}U_1\\U_2\\.\\.\\.\\\Theta_{h-1}\\\Theta_h\end{Bmatrix}_{(h-2)\times1}$

and the matrices R, Q, P are global matrices corresponding to the coefficients $\begin{bmatrix}[R_{11}]&[R_{12}]\\[R_{21}]&[R_{22}]\end{bmatrix}$, $\begin{bmatrix}[Q_{11}]&[Q_{12}]\\[Q_{21}]&[Q_{22}]\end{bmatrix}$ and $\begin{bmatrix}[P_{11}]&[P_{12}]\\[P_{21}]&[P_{22}]\end{bmatrix}$ of element Eq. (2.4.10), respectively.

2.5 Discretization in Time

Now, to obtain the complete solution of Eq. (2.4.14), further the finite element approach is used for the time domain. For this, the time domain is divided into the nodes of length $2\Delta t$ with nodal unknowns $\Omega_{k-1,}\, \Omega_{k,}\, \Omega_{k+1}$ and the shape functions M_1, M_2, and M_3. Therefore, the function Ω for interval $[t_{k-1}, t_{k+1}]$ can be approximated as (Stasa (1985))

$$\Omega = M_1\Omega_{i-1} + M_2\Omega_i + M_3\Omega_{i+1}, \tag{2.5.1}$$

where the shape functions are assumed in the forms

$$M_1(t) = -\frac{1}{2}p(1-p),\ M_2 = (1+p)(1-p),\ M_3 = \frac{1}{2}p(1+p), \tag{2.5.2}$$

and

$$p = \frac{t-t_i}{t_{k+1}-t_k} = \frac{t-t_k}{\Delta t} \text{ for } t_{t-1} \le t \le t_{t+1}, \tag{2.5.3}$$

so, $dp = dt/\Delta t$.

Therefore, the Eqs. (2.5.1- 2.5.3) give

$$\dot{\Omega}(t) = \frac{1}{\Delta t}\left[(-1/2+p)\Omega_{k-1} - 2p\Omega_k + (1/2+p)\Omega_{k+1}\right], \tag{2.5.4}$$

and

$$\ddot{\Omega}(t) = \frac{1}{(\Delta t)^2}\left[\Omega_{k-1} - 2\Omega_k + \Omega_{k+1}\right]. \tag{2.5.5}$$

Similarly, the vector f may be written as

$$f = M_1(t)f_{k-1} + M_2(t)f_k + M_3(t)f_{k+1}. \tag{2.5.6}$$

Now, by applying the Galerkin's approach on Eq. (2.4.14) and using Eqs. (2.5.1,

2.5.4-2.5.6), it is obtained that

$$\int_{-1}^{1} w \left\{ R\frac{1}{(\Delta t)^2}\left[\Omega_{k-1} - 2\Omega_k + \Omega_{k+1}\right] + Q\frac{1}{\Delta t}\left[(-1/2+p)\Omega_{k-1} - 2p\Omega_k + (1/2+p)\Omega_{k+1}\right] + P\left[-\frac{1}{2}p(1-p)\Omega_{k-1} + (1+p)(1-p)\Omega_k + \frac{1}{2}p(1+p)\Omega_{k+1}\right]\right\} dp$$
$$= \int_{-1}^{1} w\left(-\frac{1}{2}p(1-p)f_{k-1} + (1+p)(1-p)f_k + \frac{1}{2}p(1+p)f_{k+1}\right) dp, \tag{2.5.7}$$

where w is the weight function and f_{k-1}, f_k, f_{k+1} are the load vectors at nodal points of time element. All shape functions (M_1, M_2, M_3) can be considered as weight functions.

It has been verified that M_3 shows the most favorable stability and accuracy characteristics (see the book by Stasa (1985)). So, here we have considered M_3 as weight function and hence the Eq. (2.5.7) yields

$$F_1\Omega_{k+1} = F_2\Omega_k + F_3\Omega_{k-1} + G, \tag{2.5.8}$$

where

$$F_1 = R\int_{-1}^{1} M_3 dp + D\Delta t\int_{-1}^{1} M_3(1/2+p)dp + P(\Delta t)^2\int_{-1}^{1}\frac{1}{2}M_3 p(1+p)dp, \tag{2.5.9}$$

$$F_2 = 2R\int_{-1}^{1} M_3 dp + 2D\Delta t\int_{-1}^{1} M_3 p dp + P(\Delta t)^2\int_{-1}^{1}\frac{1}{2}M_3(1-p)(1+p)dp, \tag{2.5.10}$$

$$F_3 = -R\int_{-1}^{1} M_3 dp - D\Delta t\int_{-1}^{1} M_3(-1/2+p)dp + P(\Delta t)^2\int_{-1}^{1}\frac{1}{2}M_3 p(1+p)dp, \tag{2.5.11}$$

$$G = -\left[\int_{-1}^{1} \frac{1}{2} M_3 p(1-p)dp\right](\Delta t)^2 f_{k-1} + \left[\int_{-1}^{1} M_3(1+p)(1-p)dp\right](\Delta t)^2 f_k \quad (2.5.12)$$
$$-\left[\int_{-1}^{1} \frac{1}{2} M_3 p(1+p)dp\right](\Delta t)^2 f_{k+1}.$$

Further, by some detailed manipulations, the Eqs. (2.5.9-2.5.12) are reduced to

$$F_1 = R + \frac{3}{2}Q\Delta t + \frac{4}{5}P(\Delta t)^2, \quad (2.5.13)$$

$$F_2 = 2R + 2Q\Delta t - \frac{2}{5}P(\Delta t)^2, \quad (2.5.14)$$

$$F_3 = -R - \frac{1}{2}Q\Delta t + \frac{1}{5}P(\Delta t)^2, \quad (2.5.15)$$

$$G = \left[-\frac{1}{5}f_{k-1} + \frac{2}{5}f_k + \frac{4}{5}f_{k+1}\right](\Delta t)^2. \quad (2.5.16)$$

Hence, the Eq. (2.5.8) together with Eqs. (2.5.13-2.5.16), yields an explicit form of system of equations, and by using this explicit form, the value of Ω_{k+1} can be determined if the nodal unknowns Ω_k and Ω_{k-1} are known. For the first iteration at $k = 1$, we need to calculate Ω_1. For that, the Crank-Nicholson method is applied, which can be given as

$$\left[\frac{2}{\Delta t}R + Q + \frac{\Delta t}{2}P\right]\Omega_1 = \left[\frac{2}{\Delta t}R + Q - \frac{\Delta t}{2}P\right]\Omega_0 + 2R\dot{\Omega}_0 + \frac{\Delta t}{2}\left[f_0 + f_1\right]. \quad (2.5.17)$$

Now, the values of Ω_0 and $\dot{\Omega}_0$ are known from the initial conditions and f_1, f_2 are known as load vectors. Now, all the unknowns can be determined by using the iterative scheme given by Eqs. (2.5.8) and (2.5.17). This completes the theoretical development of the solution method for the present problem.

It must be pointed out that the trans-FEM method can also be used to formulate the solution for the time domain (see the refs. Bagri and Eslami (2008); Kothari and Mukhopadhyaya (2013)). In the trans-FEM method for coupled dynamical problems, the Laplace transform is applied for the time domain to get the solution of the problem in the Laplace transform domain and further a numerical inversion scheme of Laplace

transformation (like the methods of Honig and Hirdes (1984), Bellman et al. (1966), Stehfest (1970) etc.) can be used to derive the solution in the real time domain. Here the solutions obtained by the Trans-FEM method are compared with the present results and a perfect match in the behaviour of all field variables observed for both trans-FEM and present FE approach.

2.6 Numerical Results

Now, for implementation of the method, computer programming code using MATLAB is developed to solve the problem, as mentioned in the previous section. The solution to the problem is studied by computing the temperature, displacement, and stress distributions inside the hollow disk of a metallic medium under consideration of initial and boundary conditions. The reference temperature is taken to be $T_0 = 293K$. The materialistic parameters are considered for copper metal in SI unit as (Sherief and Salah (2005))

$\lambda = 7.76 \times 10^{10}\,\mathrm{kg\,m^{-1}}.s^{-2},\ \mu = 3.86 \times 10^{10}\,\mathrm{kg\,m^{-1}s^{-2}}\ \rho = 8954\,\mathrm{kg\,m^{-3}}$

$c_E = 383.1\,\mathrm{m^2\,K^{-1}\,s^{-2}},\ \alpha_t = 17.8 \times 10^{-6}\,\mathrm{K^{-1}},\ \ K = 8886.73\,\mathrm{kg\,m\,K^{-1}\,s^{-3}}$

Also, the time domain is discretized in the step size of equal length $\Delta t = 0.05$ and the dimensionless values of inner and outer radii of the disk are assumed to be 1 and 10, respectively.

The dimensionless value of heat flux delay parameters is considered as $t_q = 0.03$ and the relaxation parameters are taken to $t_2 = 0.03$, $t_1 = 0.05$. In the formulation of the finite element equation, the general case is considered, but the linear Lagrangian polynomials are assumed as shape functions for computation. For the spatial element, the hollow disk is divided into the 100 nodes of equal length along the radial direction and time domain is taken from 0 to 5. Here, the computation is performed for 100 time steps.

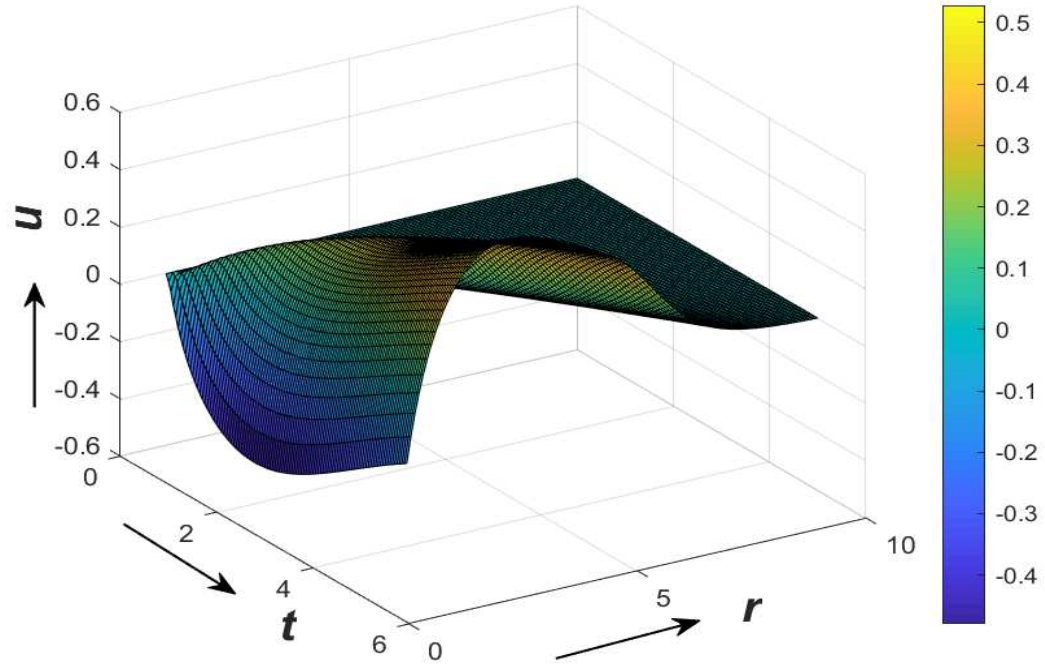

Figure 2.6.1: Variation of displacement (u) with r and t under GL theory

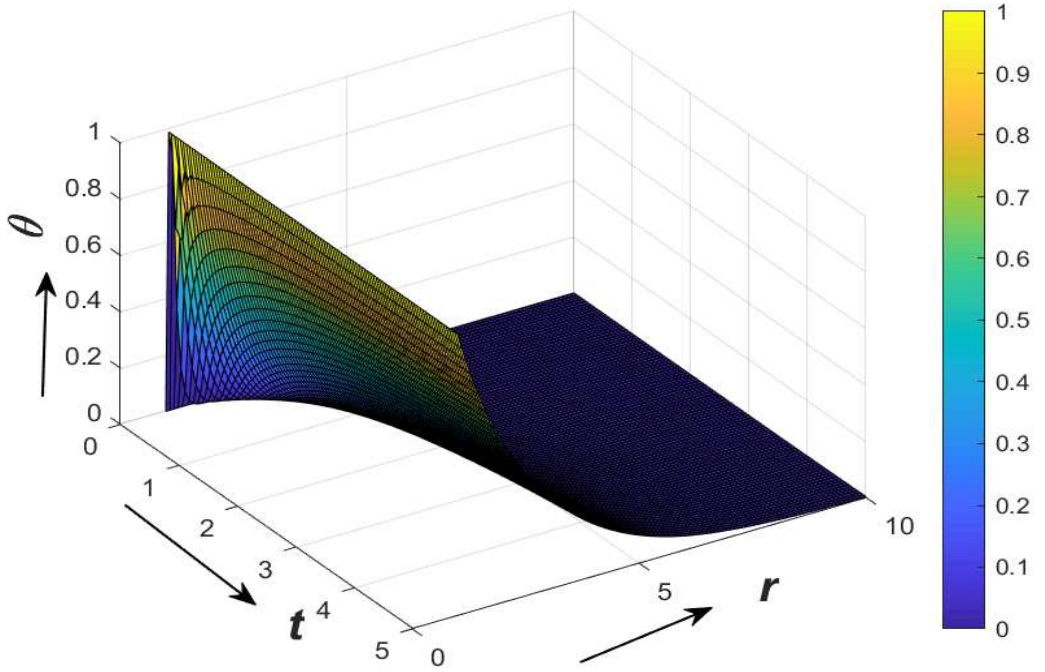

Figure 2.6.2: Variation of temperature (θ) with r and t under GL theory

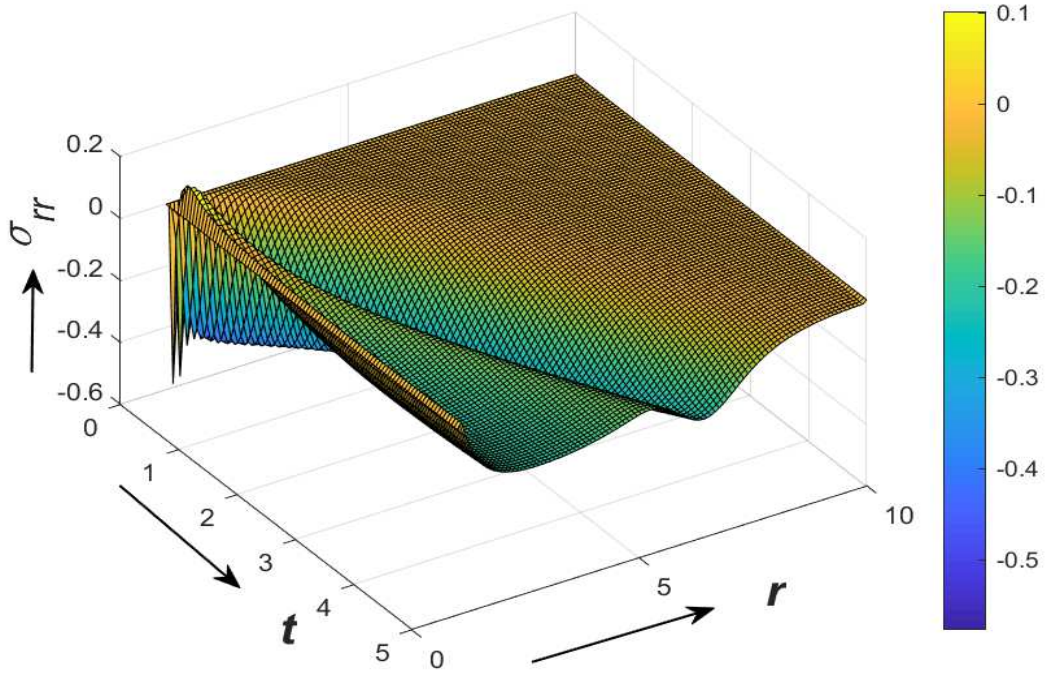

Figure 2.6.3: Variation of radial stress (σ_{rr}) with r and t under GL theory

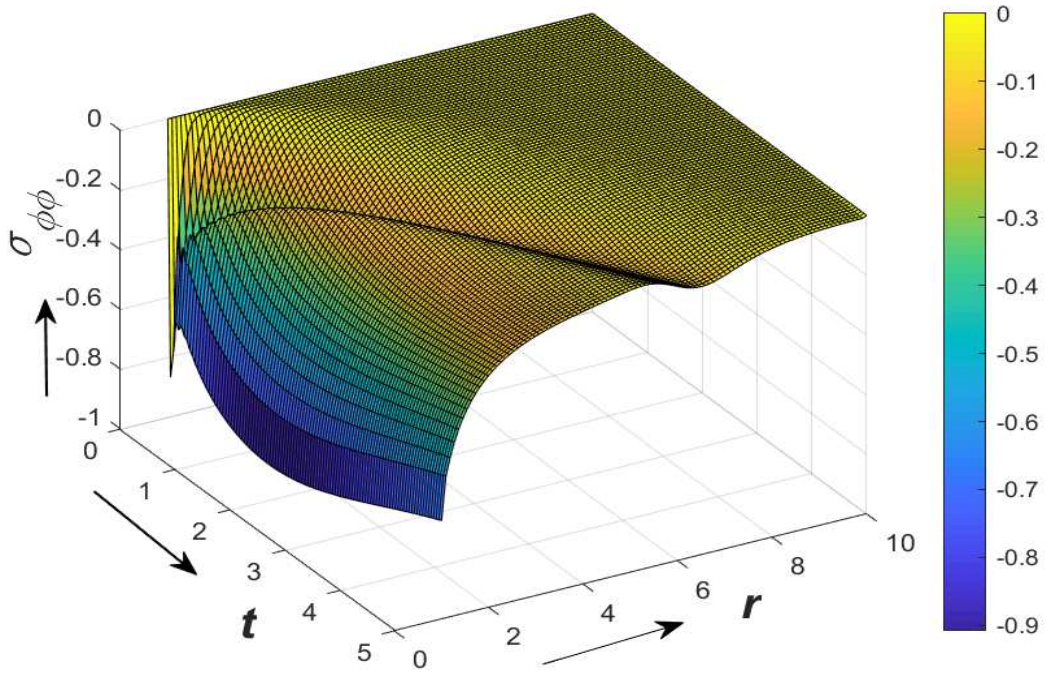

Figure 2.6.4: Variation of circumferential stress ($\sigma_{\phi\phi}$) with r and t under GL theory

The Figs. 2.6.1-2.6.4 represent the variations of the field variables under temperature-rate dependent theory (i.e., displacement, temperature, radial and circumference stresses) with respect to time and space using 3D plots.

Figure 2.6.1 clearly shows that displacement is zero at $t = 0$ and it grows up with time. The displacement starts growing from negative values at $r = 1$ to attain a maximum value after some distance from the inner boundary and then decreases to zero. The peak value of the displacement as well as the region of influence is increasing with time. However, it shows a finite domain of influence.

Figure 2.6.2 represents the temperature variation and indicates that the temperature starts decreasing from 1 to zero with space. The effective domain of influence increases with time. For example, at $t = 1.2$, the temperature reaches to zero value near $r = 2.9$, while for $t = 2.0$, it becomes zero at $r = 3.6$. In the Fig. 2.6.3, the radial stress (σ_{rr}) is plotted for various times and radial grids. At the inner boundary, it is zero and is oscillatory in nature nearer to the inner boundary. The radial stress is compressive near the region of inner boundary and becomes tensile while reaching towards the outer boundary; finally, this field becomes zero. The region of influence increases with time. The circumferential stress ($\sigma_{\phi\phi}$) is plotted in Fig. 2.6.4, displaying that $\sigma_{\phi\phi}$ starts growing up from its minimum absolute value (at $r = 1$) to a local maximum and then again after a local minimum it increases to zero w.r.t. radial distance. Also, with the increment of time, $\sigma_{\phi\phi}$ is taking the larger distance to reach its minimum and maximum values. However, this stress is fully compressive in nature.

Figures 2.6.5-2.6.8 show the comparison of solutions of the present problem obtained under two different thermoelasticity theories. It is noticed that all the field variables have a similar trend of behaviour under both the theories. However, the thermal shock at boundary has the prominent influence under the temperature-rate dependent theory and the effected region for each field under the temperature-rate dependent theory is larger than LS thermoelasticity theory.

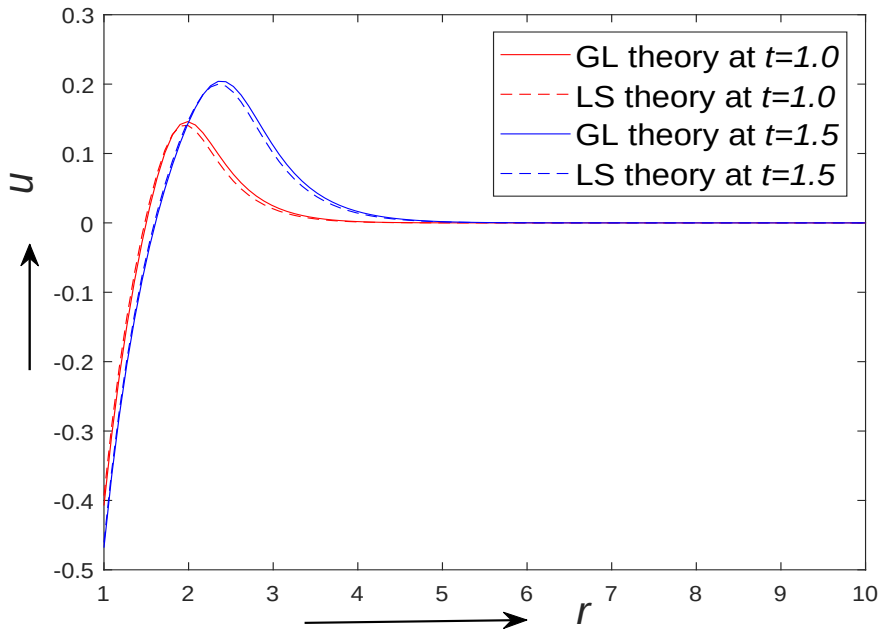

Figure 2.6.5: Distribution of displacement (u) under GL and LS theories at $t = 1.0, 1.5$

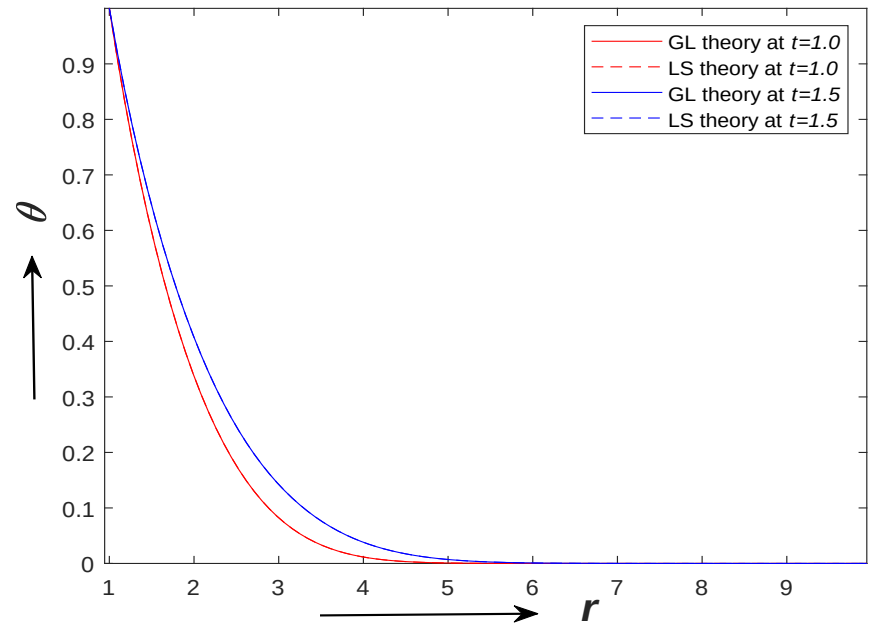

Figure 2.6.6: Distribution of temperature (θ) under GL and LS theories at $t = 1.0, 1.5$

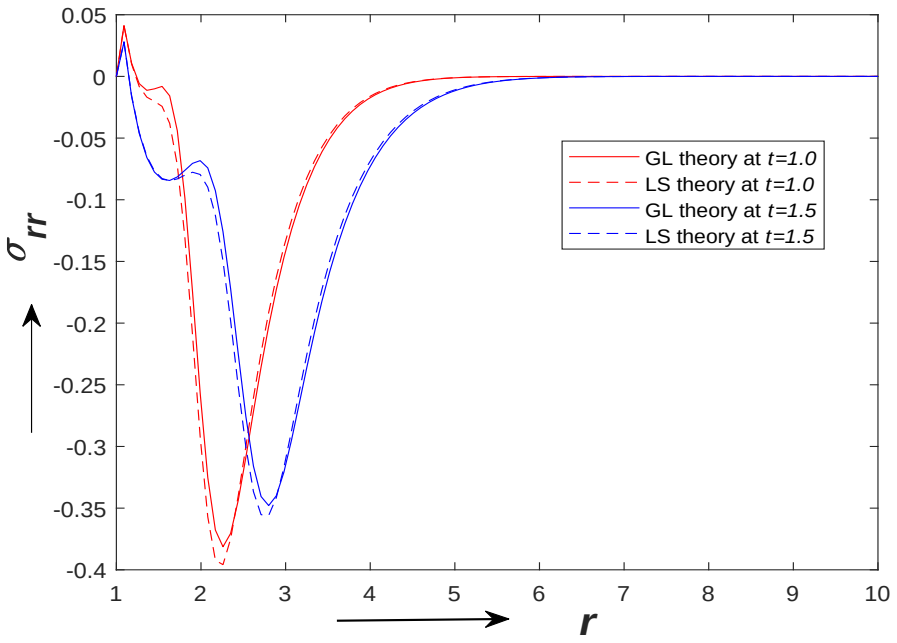

Figure 2.6.7: Distribution of radial stress (σ_{rr}) under GL and LS theories at $t = 1.0, 1.5$

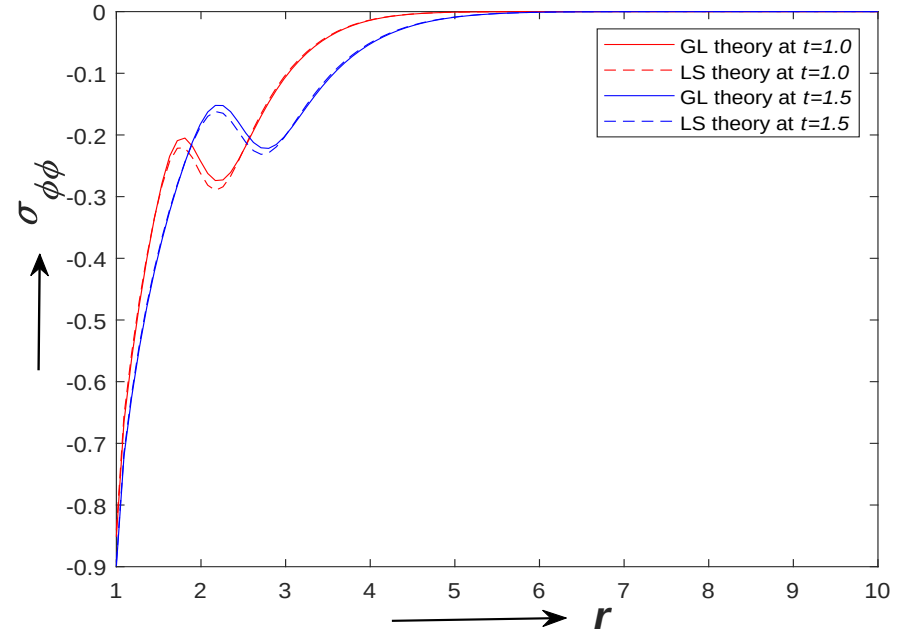

Figure 2.6.8: Distribution of circumferential stress ($\sigma_{\phi\phi}$) under GL and LS theories at $t = 1.0, 1.5$

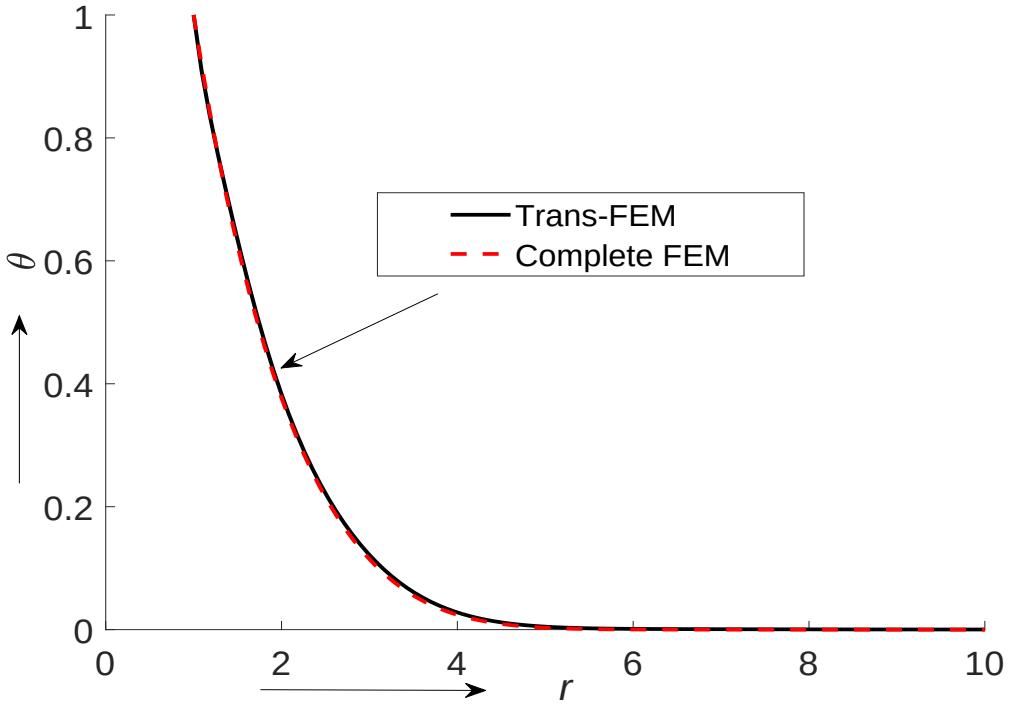

Figure 2.6.9: Temperature distribution at $t = 0.39$ for solutions obtained using trans-FEM and Complete FEM method

To validate of the present results, we have compared our solution of the problem with the corresponding solution obtained by employing the trans-finite element method, which involves the Laplace transform technique for the time domain and the numerical inversion of Laplace transform by a suitable numerical method. Here, the method given by Bellman et al. (1966) is followed for the numerical inversion of the Laplace transform. It is noted that the results obtained by the present scheme of a complete finite element method match perfectly with corresponding results obtained by the trans-finite element method. Particularly, the results of the temperature field are shown at two different times in Figs. 2.6.5-2.6.6. The black colour is used to show results for the trans-FEM method, and the red colour is used to represent the solution obtained under the complete finite element method. The similar trend of variation in the field variables and a perfect match in plots validate our results and successful implementation of the complete finite element method. Hence, any problem on coupled thermoelasticity can be solved by

using the approach as discussed in the present chapter. This approach avoids the use of the Laplace transform method and simplifies the method for the numerical solution of the problem at any time.

2.7 Conclusion

This chapter has attempted to investigate the problem of a hollow disk under linear coupled thermoelasticity based on the GL model for a homogeneous and isotropic elastic solid. A complete FEM scheme is applied to get the solution of the problem. In this process, the finite element equations for the present problem are derived for the space domain and time domain by discretizing the basic equations in space as well as in time. The validation of the results is also tested by using a well established trans- finite element method. As the trans-FEMs involve numerical inversion of Laplace transform, therefore to apply this approach, one needs to calculate the stiffness matrix for various values of the Laplace transform parameter to obtain the solution at different time steps. Hence, one major achievement of this chapter is that it provides an alternative method of solution based on finite element approach that can be more advantageous as compared to the trans-FEM method to solve the coupled thermodynamical problems as it reduces the computational complexity involved in the trans-FEM method. Another goal of the present study is to reveal a comparative analysis of solutions of the present problem obtained under two different thermoelasticity theories. It is noticed that there is a significant difference in the predictions for the behaviour of field variables by LS and GL theories. Specially, the effect of the thermal shock at the boundary has prominent influence under the temperature-rate dependent theory (GL theory) and the domain of influence under the temperature-rate dependent theory is larger as compared to LS thermoelasticity theory.